OXFORD

ORIGINAL ARTICLE

Skin Biopsy as a Novel Diagnostic Aid in Immune-Mediated Neuropathies

Young Gi Min (iD), MD, Woohee Ju, MD, Ye-Eun Ha, BS, Jae-Jun Ban, PhD, Je-Young Shin, MD, Sung-Min Kim, MD, PhD, Yoon-Ho Hong, MD, PhD, Sung-Hye Park, MD, PhD, and Jung-Joon Sung, MD, PhD

Abstract

Immune-mediated neuropathies are a heterogenous group of inflammatory peripheral nerve disorders. They can be classified according to the domain where the autoimmune process begins: the internode, paranode, or node. However, conventional diagnostic tools, electrodiagnosis (EDX), and autoantibody testing do not fully address this issue. In this institutional cohort study, we investigated the value of dermal myelinated fiber analysis for target domain-based classification. Twenty-seven consecutive patients with immune-mediated neuropathies underwent skin biopsies. The sections were stained with antibodies representative of myelinated fiber domains and were scanned using a confocal microscope. Clinical and pathological features of each patient were reviewed comprehensively. Quantitative morphometric parameters were subjected to clustering analysis, which stratified patients into 3 groups. Cluster 1 ("internodopathy") was characterized by prominent internodal disruption, intact nodes and paranodes, demyelinating EDX pattern, and absence of nodal-paranodal antibodies. Cluster 2 ("paranodopathy") was characterized by paranodal disruption and corresponding antibodies. Morphological changes were restricted to the nodes in cluster 3; we designated this cluster as "nodopathy." This report highlights the utility of skin biopsy as a diagnostic aid to gain pathogenic insight and classify patients with immune-mediated neuropathies.

From the Department of Neurology, Seoul National University Hospital, Seoul, Korea (YGM, WJ, Y-EH, J-JB, J-YS, S-MK, J-JS); Department of Translational Medicine, Seoul National University College of Medicine, Seoul, Korea (YGM); Neuroscience Research Institute, Biomedical Research Institute, Seoul National University College of Medicine, Seoul, Korea (J-JB, J-JS); Department of Neurology, Seoul National University Seoul Metropolitan Government Boramae Hospital, Seoul, Korea (Y-HH); Department of Pathology, Seoul National University Hospital, Soul, Korea (S-HP).

Send correspondence to: Jung-Joon Sung, MD, PhD, Department of Neurology, Seoul National University Hospital, Department of Translational Medicine, Seoul National University College of Medicine, 101 Daehangno, Jongnogu, Seoul 03080, Korea; E-mail: jjsaint@snu.ac.kr.

Key Words: Diagnostics, Immune-mediated neuropathies, Immunohistochemistry, Myelinated nerve fiber, Neuropathology, Skin biopsy.

INTRODUCTION

Immune-mediated neuropathies are a heterogenous group of autoimmune disorders involving the peripheral nervous system (PNS) (1–7). Diagnosis is usually made by considering clinical phenotypes, time courses, and the presence of pathogenic autoantibodies. Representative examples are Guillain-Barre syndrome (GBS), chronic inflammatory demyelinating polyradiculoneuropathy (CIDP), multifocal motor neuropathy (MMN), and antimyelin-associated glycoprotein (MAG) neuropathy (5–8). Traditionally, immune-mediated neuropathies are divided into 2 electrophysiological categories: axonal or demyelinating.

Recently, dysfunction or disruption of the nodal region has been recognized as the core pathogenesis in some immune-mediated neuropathies. Axonal GBSs are now understood as due to acute autoimmune attacks around the nodal region (9–12). Neuropathies with IgG4 antibodies to nodal/paranodal proteins are no longer classified as CIDP and are now considered to be a distinct entity called autoimmune nodopathies (5). Adding to the complexity, Oh et al (13) suggested the concept of chronic inflammatory axonal polyneuropathy (CIAP), an axonal counterpart of CIDP. In this regard, a new classification system based on the target domains of myelinated fibers has been proposed: the node, paranode, juxtaparanode, and internode (4).

Autoantibodies are useful biomarkers for this purpose (14–19). However, antibodies to nodal-paranodal proteins such as neurofascin-155 IgG4 are not widely available. Moreover, most target antigens remain unknown. The role of electrodiagnosis (EDX) is even more limited, as nodo-paranodopathy exhibits significant overlap with classical axonopathies or demyelinating neuropathies in terms of electrophysiological changes. Dysfunction of voltage-gated sodium channels at the node of Ranvier may delay the generation of action potentials leading to significant conduction slowing

into the "demyelinating range" (10, 11, 19). Where axonal degeneration may follow nodal immune attack, EDX of nodo-paranodopathy can mimic that of classical axonopathy. Therefore, novel diagnostic aids that clarify individual pathogenesis are needed.

Compared to peripheral nerves, the skin is an easily accessible source of both unmyelinated and myelinated nerve fibers (20–24). Currently, small fiber neuropathy is the most common indication for skin biopsy, with intraepidermal nerve fiber density (IENFD) being the diagnostic standard (2). Over the last decade, research has progressed to allow for the evaluation of the morphology of dermal myelinated fibers in diabetic neuropathy, Charcot-Marie-Tooth disease, GBS, and CIDP (25–28). Several morphometric parameters have been discovered: density of unmyelinated and myelinated fibers/bundles, abnormal elongation of nodes and paranodes, internodal shortening, and segmental demyelination (20, 22, 24–28). To our knowledge, few studies have employed skin biopsy to address the heterogeneity of immune-mediated neuropathies.

We hypothesized that the molecular pathology of dermal myelinated fibers may suggest which domain is primarily targeted by autoimmune responses in each patient. The sections were stained with antibodies to each myelinated fiber domain and then analyzed using a confocal microscope. Quantitative morphometric parameters for each domain were then subjected to clustering analysis, which stratified patients into 3 groups. Clinical and pathological features of each cluster were reviewed in detail. This report highlights the utility of skin biopsy as a diagnostic aid to gain pathogenic insight and classify immune-mediated neuropathies.

MATERIALS AND METHODS

Patients

Ethical approval for this study was provided by the Institutional Review Board of Seoul National University Hospital (IRB no. 1906-160-1045). The study was conducted in compliance with the principles of the Declaration of Helsinki. All participants provided written informed consent prior to participating in the study.

Between October 2020 and July 2021, 27 consecutive patients admitted to the Department of Neurology of Seoul National University Hospital for diagnosis or treatment of immune-mediated neuropathies were prospectively recruited. Patients were confirmed as having immune-mediated neuropathies posteriori when they met the following criteria: (i) immunologic or pathologic evidence of autoimmune origin; (ii) positive response to immunotherapy; and (iii) absence of alternative causes. Patients who met the corresponding criteria were labeled as GBS, CIDP, MMN, or anti-MAG neuropathy (5–8, 29).

Skin Biopsy and Immunohistochemistry

All participants underwent a 4-mm punch biopsy from the distal leg (10 cm proximal to the lateral malleolus) and the proximal thigh (20 cm distal to the iliac crest). The samples were washed briefly with phosphate-buffered saline (PBS)

and fixed in Zamboni's solution for up to 24 hours at 4°C. The specimens were then embedded in optimal cutting temperature medium and cut into 50-μm thick sections using a cryotome (CM1860; Leica, Germany). Free-floating sections were incubated with primary antibodies for 24 hours at room temperature. On the following day, the sections were washed twice in PBS and incubated with secondary antibodies for 1 hour at room temperature. The sections were then washed with PBS and mounted onto slides. The antibody sources and dilutions are listed in Supplementary Table S1.

Triple immunostaining was performed using 2 combinations of antibodies: (i) protein gene product 9.5 (PGP9.5; GTX10410, GeneTex, Irvine, CA, 1:500, axon), myelin basic protein ([MBP]; GTX76114, GeneTex, 1:600, myelin), and voltage-gated sodium channel (Nav; S8809, Sigma, St Louis, MO, 1:100, node of Ranvier); or (ii) MBP, Nav, and contactin-associated protein (Caspr; ab34151, Abcam, Cambridge, UK, 1:100, paranode) (Supplementary Table S1). Three distal leg sections for each combination were analyzed per patient. In 9 patients whose myelinated fibers were insufficient for further analysis (less than 8 internodes, 30 nodes or paranodes), 3 proximal leg sections were additionally stained with the first antibody combination.

Morphometric Analysis

The sections were scanned using a confocal microscope (LSM900; Zeiss, Oberkochen, Germany). IENFD and dermal myelinated nerve bundle density were measured from 3 nonconsecutive distal leg sections stained with PGP9.5 and MBP (in first combination) at 2.5× objective, as described elsewhere (2, 20–28). A dermal myelinated bundle was defined as a group of more than 5 nerve fibers that contains at least 1 myelinated fiber (24). Whether a patient's IENFD was below the normal limit was determined according to age and sex-adjusted reference values (2). All nodes, paranodes, or internodes observed were imaged at 20× objective. Z-stack images were acquired at 1-μm increments.

The quantitative parameters of dermal myelinated nerve fiber morphology were measured as described elsewhere (20, 22–28). Briefly, internodal length is the length of the myelin segment (MBP). Nodal gap length refers to the MBP-flanked, PGP9.5-positive region surrounded by internodes at both ends. Paranodal length is the length of Caspr-stained bands located as a pair, with a node in between. In each patient, the results were presented in 2 approaches: the mean of measured values (μm) and the proportion of abnormal measured values (%). Reference values were defined as 2 standard deviations from the mean of intra-laboratory controls (296 nodes, 258 paranodes, and 72 internodes from 15 healthy controls). Accordingly, nodes > 4.81 μm and internodes < 42.9 μm were determined to be abnormal. Paranodes were considered abnormal if their length exceeded 7.16 μm or Caspr staining was totally lost (20, 27). Segmental demyelination was defined as the segmental absence of myelin sheath (MBP) with intact axonal continuity (PGP9.5) (27).

Representative confocal images were also presented to visualize morphological abnormalities of dermal myelinated fibers. Slice images acquired at 1-μm increment were pro-

jected into a single reconstructed 2D image. The fluorescence intensities of MBP, Caspr, and Nav (second combination) were measured to analyze the molecular organization of the nodal region. Along the node, a curvilinear-shaped region of interest was drawn by blinded examiners (Y.-E.H. and J-.J.B.). Fluorescence intensity was measured using ZEN 2.0 software (Oberkochen, Germany). Gain values were maintained constant throughout the study to minimize experimental errors.

Cluster Analysis

Cluster analysis is a statistical technique that groups objects into several clusters that share similar patterns of observations (30). In this study, we used agglomerative hierarchical clustering to identify subgroups that share similar dermal myelinated fiber abnormalities. Normalized data of the proportion of elongated nodes, abnormal paranodes, and short internodes were used. The Pearson correlation distance of the normalized data was used as the dissimilarity measure. The average linkage method was used to define the inter-cluster distances. The optimal number of clusters was determined using the NbClust R package, which provides a total of 30 indices evaluating how well the clustering results fit the dataset (31). The number of clusters identified by most indices was considered optimal. Patients with severe axonal loss, that yielded fewer than 10 nodes, 10 paranodes, or 5 internodes, were excluded from the analysis.

Electrodiagnosis

The nerve conduction study was conducted through conventional procedures using Nicolet EDX with Viking software, as described previously (32). Whether patients met the EDX criteria for demyelination was assessed according to the European Academy of Neurology/Peripheral Nerve Society (EAN/PNS) criteria 2021, or the Rajabally's criteria, as appropriate (5, 33). As for patients with chronic-onset neuropathies, EDX data were classified as exhibiting demyelination, weakly supportive of demyelination, or axonal subtype. EDX data of GBS patients were classified as demyelination, axonal, or unclassifiable subtype.

Statistical Analysis

Variables are expressed as medians (interquartile range) or number of patients (percentage). Comparison between clusters was performed using the Fisher exact test for categorical variables and the Kruskal-Wallis test for continuous variables. We used the Pearson correlation coefficient to assess the correlation between quantitative parameters from skin biopsy. Statistical significance was set at a 2-tailed $p < 0.05$. All statistical analyses were performed using R version 4.1.1 for Windows.

RESULTS

Study Participants

Twenty-seven patients underwent skin biopsies without complications. Two patients were excluded because they had amyotrophic lateral sclerosis and Lambert-Eaton myasthenic syndrome, respectively. The clinical diagnoses of the remaining patients were as follows: CIDP (n = 10), GBS (n = 8), anti-MAG neuropathy (n = 3), MMN (n = 1), cauda equina syndrome (n = 1), chronic ataxic neuropathy with disialosyl antibodies (CANDA, n = 1), and CIAP (n = 1) (14, 34, 35). Based on the EAN/PNS 2021 guideline, every patient was under diagnostic certainty of "CIDP," while none was under "possible CIDP" (5). One patient with cauda equina syndrome exhibited albumino-cytologic dissociations, no structural lesions, and improvement after immunotherapy; this patient was therefore considered to have disease of autoimmune origin.

Cluster Analysis

A total of 841 nodes, 841 paranodes, and 218 internodes from 25 patients were analyzed. Two subjects (1 GBS and 1 CIDP) with few measurable fibers were excluded from the cluster analysis; their myelinated bundle densities (/mm^2) and sural nerve action potentials (µV) were both 0. Agglomerative hierarchical clustering was applied to the dataset of the remaining patients (n = 23). The optimal number of clusters was determined to be 3 (Supplementary Data Fig. S1). Figure 1 shows a heatmap displaying the morphological profiles of dermal myelinated fibers, the presence of autoantibodies, and the electrophysiologic categories for each cluster.

Baseline Demographic and Clinical Characteristics

The Table shows a comparison of the detailed clinical features, serum autoantibodies, EDX patterns, and skin biopsy-driven parameters of each cluster. The age and sex ratios were comparable between clusters (both p = 0.7). Autoantibodies against MAG or gangliosides were most common in cluster 2 (63%), followed by cluster 3 (14%) (p = 0.026). The distribution of EDX patterns did not differ statistically between the clusters (p = 0.2). However, the axonal type was most common in cluster 2 (50%), whereas it was absent in cluster 1 (0%). Patients in clusters 1 (75%) and 3 (71%) frequently showed an EDX pattern supportive of demyelination, as compared to those in cluster 2 (38%).

Comparison of Quantitative Skin Biopsy-Driven Parameters

IENFD values were comparable between clusters (p = 0.7). A significant proportion of patients had below normal IENFD: 50, 75, and 71% in cluster 1, 2, and 3, respectively. No significant difference was noted across clusters (p = 0.6). The density of dermal myelinated bundles was low in cluster 2 compared to the other clusters (p = 0.024). Analysis of nodal gaps, paranodes, and internodes revealed distinct patterns of morphological alterations in each cluster (Table). The proportion of elongated nodes was higher in cluster 2 (median 19%) and cluster 3 (median 19%) than in cluster 1 (median 11%) (p = 0.039). Abnormal paranodes were common in cluster 2 (median 17%) but not in the others (median 5–6%) (p = 0.005). Abnormally shortened internodes were
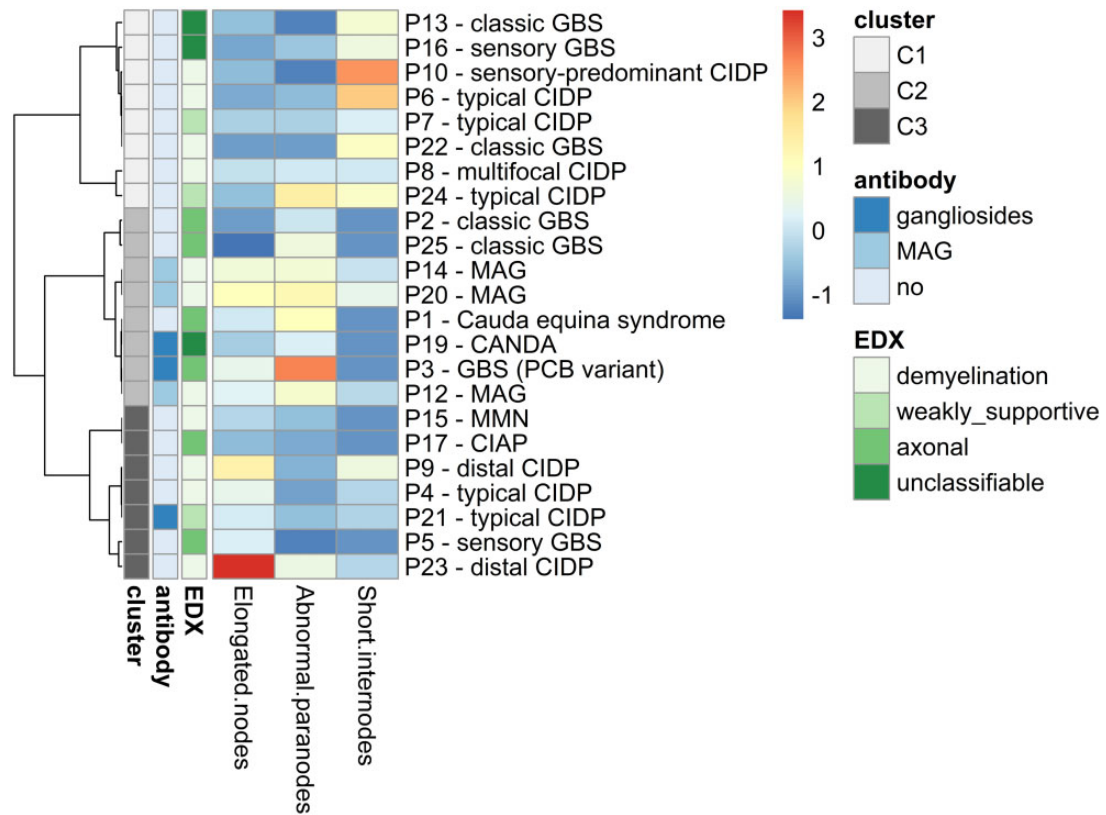
FIGURE 1. A heatmap displaying the clinical and pathological profiles. Results of autoantibody testing, electrodiagnosis, and the cluster membership are indicated by column annotations. Clinical diagnosis and the patient number are expressed as row annotations. EDX, electrodiagnosis; GBS, Guillain-Barre syndrome; CIDP, chronic inflammatory demyelinating polyradiculoneuropathy; PCB, pharyngeal-cervical-brachial; MMN, multifocal motor neuropathy; CIAP, chronic inflammatory axonal polyneuropathy; MAG, myelin-associated glycoprotein.

most common in cluster 1 (median 26%) (cluster 2: median 0%, cluster 3: median 11%) ($p = 0.001$). In contrast to the "proportion of abnormal values," no statistical differences were seen when the "mean of every measured value" was compared (nodal gap length: $p = 0.5$, paranodal length: $p = 0.15$, internodal length: $p = 0.2$). The distribution of all measurements (not averaged by the patient) is shown in Supplementary Data Figure S2.

Morphological Alterations of Myelinated Nerve Fiber Domains

Figure 2 shows representative examples of internodal disruption, which is predominantly found in cluster 1. Figure 2A is the normal structure of a dermal myelinated bundle, which contains 1 myelinated fiber (MBP) and numerous unmyelinated fibers (PGP9.5). Internodes of sufficient length (arrows) are connected at narrow nodal gaps. Segmental absence of myelin sheath on an intact axon, referred to as segmental demyelination, is shown in Figure 2B (arrowheads). The abnormal shortening of internodes ($<42.9 \mu m$) is also seen frequently (Fig. 2B, arrows, also see the Table). Figure 2C shows selective fragmentation of myelin sheaths (arrowheads), and spared nodes (dashed circles) and axons, which were noted in GBS patients in cluster 1. Focal

swelling of internodal myelin (tomaculous appearance) is observed in cluster 1, as well as in patients with anti-MAG neuropathy (cluster 2) (Fig. 2D, asterisk).

Figure 3 displays structural organization along the node of Ranvier, in terms of fluorescence intensity profiles of MBP (red), Caspr (green), and Nav (blue). Under normal conditions (Fig. 3A), sodium channels (asterisk) are highly concentrated within a short distance. Next to the sodium channel cluster is a pair of Caspr bands and the myelin sheath. Figure 3B, C shows patterns of paranodal disruption, which are exclusively found in cluster 2 patients: the extensive spreading of Caspr into the juxtaparanodes and internodes (Fig. 3B, dashed arrows; also see Supplementary Data Fig. S2) or loss of Caspr immunoreactivity (Fig. 3C, dashed arrow). Nodal disruption, such as loss of Nav immunoreactivity, (Fig. 3B, asterisk) is commonly found in clusters 2 and 3. In contrast, the structural integrity of the nodes and the paranodes was relatively preserved in cluster 1, although the fluorescence intensities of MBP were generally low (Fig. 3D, arrows).

DISCUSSION

Recent understanding of the pathogenesis of immune-mediated neuropathies has highlighted a need for more systematic classification (4, 10, 11). Nerve biopsy is not recom-

TABLE. Comparison of Baseline Characteristics Between 3 Clusters

Characteristic	C1 (n = 8)	C2 (n = 8)	C3 (n = 7)	Overall p Value
Demographic characteristics				
Sex (F:M)	2:6	2:6	3:4	0.7
Age (years)	62 (55, 74)	62 (33, 73)	60 (40, 62)	0.7
Autoantibody status				0.026*
Gangliosides	0 (0%)	2 (25%)[†]	1 (14%)[‡]	
MAG	0 (0%)	3 (38%)	0 (0%)	
None	8 (100%)	3 (38%)	6 (86%)	
Electrodiagnosis				0.2
Axonal	0 (0%)	4 (50%)	2 (29%)	
Demyelination	4 (50%)	3 (38%)	4 (57%)	
Demyelination (weakly supportive of)	2 (25%)	0 (0%)	1 (14%)	
Unclassifiable	2 (25%)	1 (12%)	0 (0%)	
Skin biopsy parameters				0.7
IENFD (/mm)	3.92 (2.53, 4.93)	2.97 (1.62, 4.34)	3.70 (3.16, 6.62)	0.7
Abnormal IENFD	4 (50%)	6 (75%)	5 (71%)	0.6
Myelinated bundle density (/mm^2)	0.45 (0.38, 0.66)	0.20 (0.00, 0.33)	0.34 (0.14, 0.36)	0.024*
Nodal gap length (μm)	3.42 (3.04, 3.91)	3.84 (3.15, 3.96)	3.67 (3.50, 4.22)	0.5
Elongated nodes (%)	11 (9, 12)	19 (12, 22)	19 (17, 26)	0.039*
Paranodal length (μm)	5.02 (4.39, 5.40)	5.19 (4.88, 5.70)	4.55 (4.37, 5.02)	0.15
Abnormal paranode (%)	6 (2, 8)	17 (14, 19)	5 (3, 6)	0.005*
Internodal length (μm)	62 (57, 69)	82 (64, 108)	78 (71, 81)	0.2
Short internodes (%)	26 (21, 32)	0 (0, 13)	11 (0, 12)	0.001*
Segmental demyelination[¶]	8 (100%)	3 (38%)	3 (43%)	0.022*

*p < 0.05.
[†]GQ1b IgM, GD1b, and GQ1b IgM in GBS (PCB) and CANDA patients, respectively.
[‡]GM1 IgM in a patient with CIDP diagnosis.
[¶]Segmental demyelination was determined as either present or absent.
IENFD, intra-epidermal nerve fiber density; MAG, membrane-associated glycoprotein.

mended as a routine diagnostic procedure due to its infeasibility and morbidity (5, 35). We hypothesized that nerve fibers in the skin would be a useful alternative for studying the molecular pathogenesis of immune-mediated neuropathies. Through comprehensive confocal analysis and morphometric data clustering, we show that skin biopsy can identify the domains where immune responses begin.

In cluster 1, pathological alterations were mainly seen in the internodal domain. Segmental demyelination and abnormally shortened internodes were the pathologic hallmarks, which had been reported in the sural nerves and skin of CIDP (27, 36). None of the patients in this cluster had autoantibodies to nodes or paranodes. Collectively, we speculate that this group represents "demyelinating internodopathy." Notably, morphological changes were observed even in 2 patients with unclassifiable EDX, highlighting the usefulness of skin biopsy. Another interesting finding is that abnormal IENFD was noted in a significant portion of patients, corroborating with previous reports of various demyelinating neuropathies (26, 37, 38).

Cluster 2 was characterized by the disruption of both nodes and paranodes. While the former was also common in cluster 3, the latter was specific to this cluster. Dispersion of paranodes and complete loss of Caspr staining were observed. Interestingly, similar findings have been reported in patients with IgG4 antibodies to neurofascin-155, contactin-1, and Caspr (14). In our study, 2 patients had antibodies to disialosyl gangliosides, which are expressed on paranodal axolemma (12, 39, 40). Three patients with anti-MAG neuropathy were also grouped into cluster 2. MAGs are present on terminal myelin loops (paranode) and Schmidt-Lantermann incisures (internode). Therefore, IgM antibodies to MAG widen the myelin lamellae beginning from these regions, resulting in tomaculous myelin or segmental demyelination (22, 41, 42). In line with these reports, paranodal dispersion, focal swelling of myelin sheath, and segmental demyelination were all observed in our patients (41, 42). Apart from the patients with anti-MAG neuropathy, no patient in cluster 2 showed the overlapping features of internodopathy and paranodopathy. Collectively, we speculate that cluster 2 represents "paranodopathy" and could be further divided into "nodo-paranodopathy" and "paranodo-internodopathy."

The node of Ranvier was the only domain involved in cluster 3. Nodal disruption has also been reported in the skin of patients with axonal neuropathies (20, 28). However, the magnitude of nodal disruption in these studies is much smaller than that observed in our patients; Doppler et al reported that only 0–10% of axonal neuropathy patients had any elongated nodes, accounting for 1.4% of the entire nodes. In contrast, prominent nodal elongation, ranging from 11.4% to 51.7% of
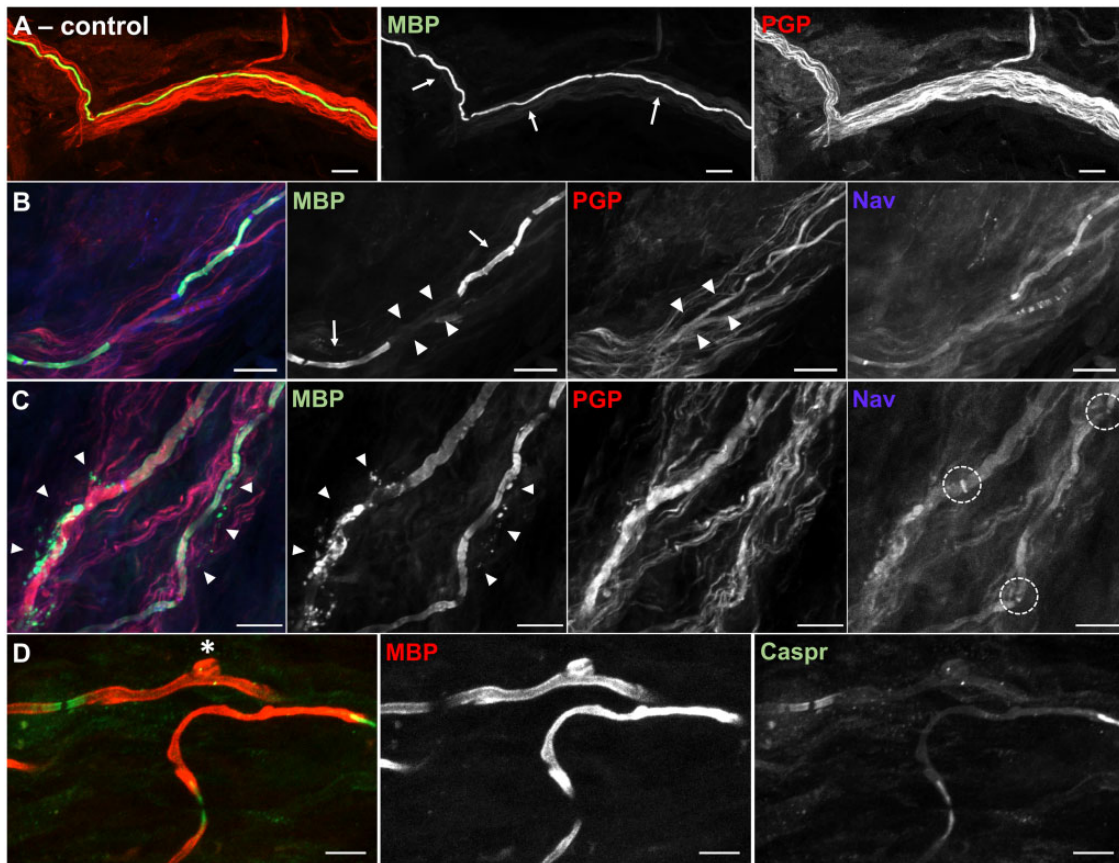
FIGURE 2. Normal **(A)** and pathological alterations of the internodes **(B–D)**. These findings are predominantly found in cluster 1. **(B)** Segmental demyelination observed in a CIDP patient. Note the absence of myelin sheath (arrowheads, MBP) with preserved axonal morphology (arrowheads, PGP). In addition, 2 internodes (arrows) adjacent to the denuded axon (arrowheads) are abnormally shortened. **(C)** Fragmentation of myelin sheaths (arrowheads, MBP) but not axons found in a patient with acute inflammatory demyelinating polyradiculoneuropathy. Note that sodium channel clusters (dashed circles, Nav) are preserved. **(D)** Focal swelling of myelin lamellae (asterisk) at the middle of an internode. These findings are noted in cluster 1, as well as in patients with anti-MAG neuropathy in cluster 2. Scale bar = 20 μm.

all nodes, was found in every patient in cluster 3. Furthermore, our patients had 1 or more objective clues for autoimmune etiology, such as inflammatory infiltrates in a sural nerve, presence of GM1 IgM antibody, or clear treatment responses. Collectively, we speculate that "nodopathy" best explains this cluster. However, whether inflammatory insults to the nodes could selectively derange sodium channels while sparing paranodal structures needs to be confirmed by further studies.

The limitations in our study should be acknowledged. Although we recruited consecutive patients in a prospective manner, the sample size was small and did not include all immune-mediated neuropathies. We did not examine IgG4 autoantibodies to nodal/paranodal glycoproteins, which might have enriched the interpretation of our results. Additionally, conventional histologic assessments such as toluidine blue staining were not performed. Lastly, the present study does not elucidate disease mechanisms at the ultrastructural level, which requires electron microscope analysis.

In summary, we performed confocal analysis of dermal myelinated fibers and parameter-driven clustering in a small institutional cohort of immune-mediated neuropathies. Our data support the utility of skin biopsy as a diagnostic aid for determining the target domain in individual patients. In particular, skin biopsy may complement 2 major limitations of EDX: early detection of nodal pathology and reliable diagnosis of demyelination in sensory nerves. Our findings need to be confirmed in future studies with more patients. In addition, it would be of interest to correlate skin biopsy findings with clinical and EDX parameters and test whether skin biopsy improves management by allowing more patients receive appropriate immunotherapy.

DATA AVAILABILITY

The data that support the findings of this study are available from the corresponding author upon reasonable request.
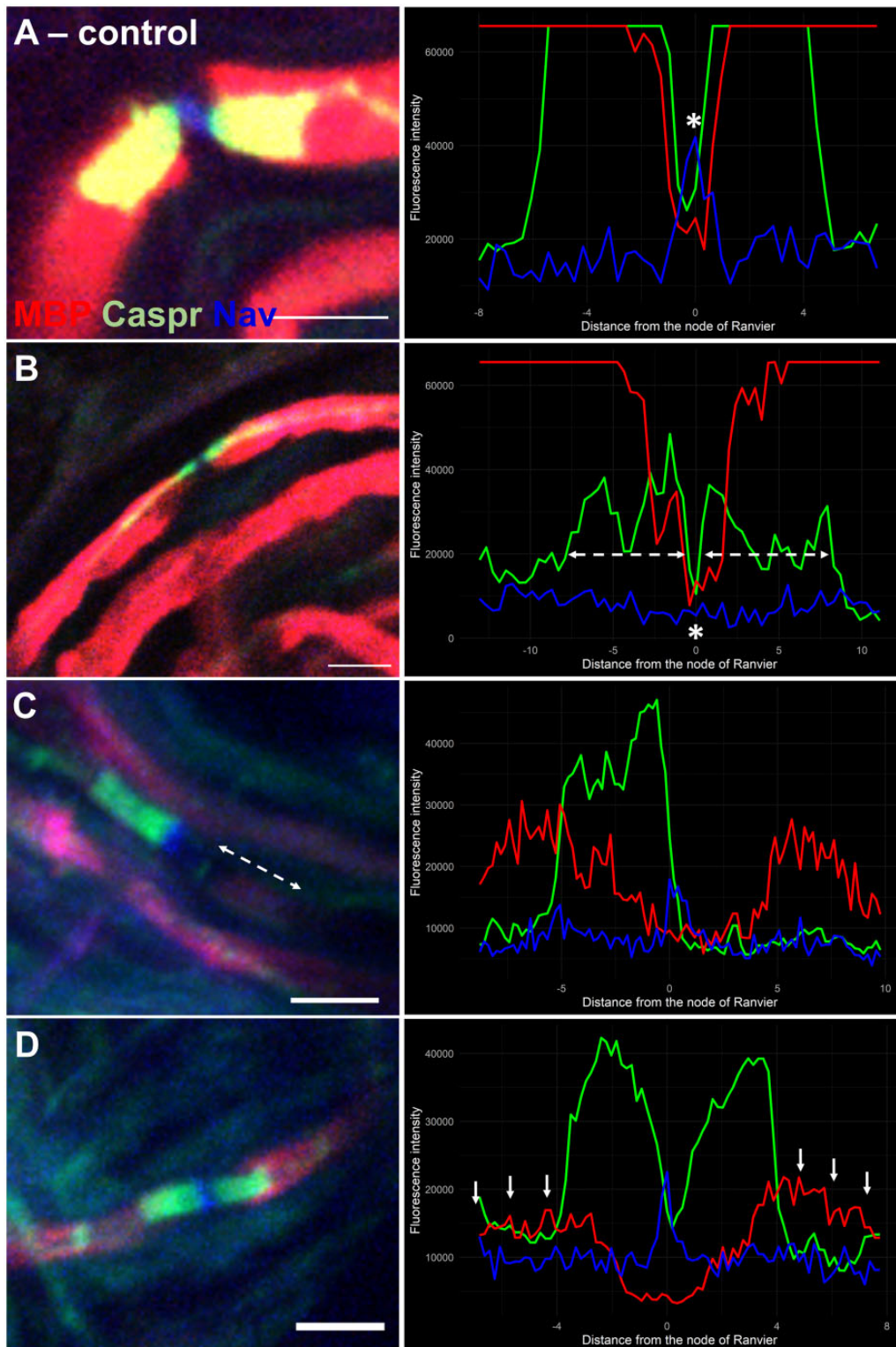
FIGURE 3. Fluorescence intensity profiles at the nodal region. **(A)** In control, sodium channels exist as a cluster (asterisk), surrounded by a pair of Caspr bands and myelin sheaths. **(B)** Loss of Nav staining (asterisk) and Caspr dispersion (dashed arrows) noted in a GBS patient in cluster 2. **(C)** Loss of Caspr staining, either unilaterally (dashed line, or bilaterally (not shown), is also found in this cluster). **(D)** Nodes and paranodes are relatively preserved in cluster 1, whereas the MBP fluorescence intensity of myelin sheaths is generally low. Scale bar = 5 μm.

REFERENCES

1. Kieseier BC, Mathey EK, Sommer C, et al. Immune-mediated neuropathies. Nat Rev Dis Primers 2018;4:31
2. Lauria G, Hsieh ST, Johansson O, et al. European Federation of Neurological Societies/Peripheral Nerve Society Guideline on the use of skin biopsy in the diagnosis of small fiber neuropathy. Report of a joint task force of the European Federation of Neurological Societies and the Peripheral Nerve Society. Eur J Neurol 2010;17:903–12.e44-9
3. Motte J, Fisse AL, Kose N, et al. Treatment response to cyclophosphamide, rituximab, and bortezomib in chronic immune-mediated sensorimotor neuropathies: A retrospective cohort study. Ther Adv Neurol Disord 2021;14:1756286421999631
4. Uncini A, Mathis S, Vallat JM. New classification of autoimmune neuropathies based on target antigens and involved domains of myelinated fibres. J Neurol Neurosurg Psychiatry 2022;93:57–67
5. Van den Bergh PYK, van Doorn PA, Hadden RDM, et al. European Academy of Neurology/Peripheral Nerve Society guideline on diagnosis and treatment of chronic inflammatory demyelinating polyradiculoneuropathy: Report of a joint Task Force-Second revision. Eur J Neurol 2021;28:3556–3583
6. Wakerley BR, Uncini A, Yuki N; GBS Classification Group. Guillain-Barre and Miller Fisher syndromes–new diagnostic classification. Nat Rev Neurol 2014;10:537–44
7. Yeh WZ, Dyck PJ, van den Berg LH, et al. Multifocal motor neuropathy: Controversies and priorities. J Neurol Neurosurg Psychiatry 2020;91:140–148
8. Steck AJ. Anti-MAG neuropathy: From biology to clinical management. J Neuroimmunol 2021;361:577725
9. He L, Zhang G, Liu W, et al. Anti-ganglioside antibodies induce nodal and axonal injury via Fcgamma receptor-mediated inflammation. J Neurosci 2015;35:6770–85
10. Oh SJ. Nodal conduction block: A unifying concept. Muscle Nerve 2021;63:178–180
11. Uncini A, Santoro L. The electrophysiology of axonal neuropathies: More than just evidence of axonal loss. Clin Neurophysiol 2020;131:2367–2374
12. Yuki N, Uncini A. Acute and chronic ataxic neuropathies with disialosyl antibodies: A continuous clinical spectrum and a common pathophysiological mechanism. Muscle Nerve 2014;49:629–35
13. Oh SJ, Lu L, Alsharabati M, et al. Chronic inflammatory axonal polyneuropathy. J Neurol Neurosurg Psychiatry 2020;91:1175–1180
14. Cortese A, Lombardi R, Briani C, et al. Antibodies to neurofascin, contactin-1, and contactin-associated protein 1 in CIDP. Neurol Neuroimmunol Neuroinflamm 2020;7:e639
15. Delmont E, Manso C, Querol L, et al. Autoantibodies to nodal isoforms of neurofascin in chronic inflammatory demyelinating polyneuropathy. Brain 2017;140:1851–1858
16. Susuki K, Rasband MN, Tohyama K, et al. Anti-GM1 antibodies cause complement-mediated disruption of sodium channel clusters in peripheral motor nerve fibers. J Neurosci 2007;27:3956–67
17. Yamagishi Y, Kuwahara M, Suzuki H, et al. Serum IgG anti-GD1a antibody and mEGOS predict outcome in Guillain-Barre syndrome. J Neurol Neurosurg Psychiatry 2020;91:1339–1342
18. Vallat JM, Mathis S, Vegezzi E, et al. Antibody- and macrophage-mediated segmental demyelination in chronic inflammatory demyelinating polyneuropathy: clinical, electrophysiological, immunological and pathological correlates. Eur J Neurol 2020;27:692–701
19. Kouton L, Boucraut J, Devaux J, et al. Electrophysiological features of chronic inflammatory demyelinating polyradiculoneuropathy associated with IgG4 antibodies targeting neurofascin 155 or contactin 1 glycoproteins. Clin Neurophysiol 2020;131:921–927
20. Doppler K, Werner C, Sommer C. Disruption of nodal architecture in skin biopsies of patients with demyelinating neuropathies. J Peripher Nerv Syst 2013;18:168–176
21. Lombardi R, Erne B, Lauria G, et al. IgM deposits on skin nerves in anti-myelin-associated glycoprotein neuropathy. Ann Neurol 2005;57:180–7
22. Provitera V, Nolano M, Pagano A, et al. Myelinated nerve endings in human skin. Muscle Nerve 2007;35:767–75
23. Provitera V, Piscosquito G, Manganelli F, et al. A model to study myelinated fiber degeneration and regeneration in human skin. Ann Neurol 2020;87:456–465
24. Doppler K, Werner C, Henneges C, et al. Analysis of myelinated fibers in human skin biopsies of patients with neuropathies. J Neurol 2012;259:1879–1887
25. Manganelli F, Nolano M, Pisciotta C, et al. Charcot-Marie-Tooth disease: New insights from skin biopsy. Neurology 2015;85:1202–8
26. Ruts L, van Doorn PA, Lombardi R, et al. Unmyelinated and myelinated skin nerve damage in Guillain-Barre syndrome: Correlation with pain and recovery. Pain 2012;153:399–409
27. Saporta MA, Katona I, Lewis RA, et al. Shortened internodal length of dermal myelinated nerve fibres in Charcot-Marie-Tooth disease type 1A. Brain 2009;132:3263–3273
28. Doppler K, Frank F, Koschker AC, et al. Nodes of Ranvier in skin biopsies of patients with diabetes mellitus. J Peripher Nerv Syst 2017;22:182–190
29. Uncini A, Yuki N. Sensory Guillain-Barré syndrome and related disorders: An attempt at systematization. Muscle Nerve 2012;45:464–70
30. Rodriguez MZ, Comin CH, Casanova D, et al. Clustering algorithms: A comparative approach. PLoS One 2019;14:e0210236
31. Charrad M, Ghazzali N, Boiteau V, et al. NbClust: an R package for determining the relevant number of clusters in a data set. J Stat Soft 2014;61:1–36
32. Min YG, Choi S-J, Hong Y-H, et al. Dissociated leg muscle atrophy in amyotrophic lateral sclerosis/motor neuron disease: The 'split-leg' sign. Sci Rep 2020;10:15661
33. Rajabally YA, Durand MC, Mitchell J, et al. Electrophysiological diagnosis of Guillain-Barré syndrome subtype: Could a single study suffice? J Neurol Neurosurg Psychiatry 2015;86:115–9
34. Garcia-Santibanez R, Zaidman CM, Sommerville RB, et al. CANOMAD and other chronic ataxic neuropathies with disialosyl antibodies (CANDA). J Neurol 2018;265:1402–1409
35. Nathani D, Spies J, Barnett MH, et al. Nerve biopsy: Current indications and decision tools. Muscle Nerve 2021;64:125–139
36. Luigetti M, Romano A, Di Paolantonio A, et al. Pathological findings in chronic inflammatory demyelinating polyradiculoneuropathy: A single-center experience. Brain Sci 2020;10:383
37. Pan CL, Tseng TJ, Lin YH, et al. Cutaneous innervation in Guillain-Barré syndrome: Pathology and clinical correlations. Brain 2003;126:386–397
38. Chiang MC, Lin YH, Tseng TJ, et al. Cutaneous innervation in chronic inflammatory demyelinating polyneuropathy. Neurology 2002;59:1094–1098
39. Miller JAL, Spyropoulos A, Jaros E, et al. Anti-GQ1b ganglioside positive Miller Fisher syndrome – Evidence of paranodal pathology on nerve biopsy. J Neuromuscul Dis 2014;1:191–195
40. Vallat J-M, Deschamps N, Taithe F, et al. Are Miller Fisher syndrome and CANDA due to a paranodopathy? J Neurol Sci 2022;438:120279
41. Kawagashira Y, Koike H, Tomita M, et al. Morphological progression of myelin abnormalities in IgM-monoclonal gammopathy of undetermined significance anti-myelin-associated glycoprotein neuropathy. J Neuropathol Exp Neurol 2010;69:1143–57
42. Kawagashira Y, Koike H, Takahashi M, et al. Aberrant expression of nodal and paranodal molecules in neuropathy associated with IgM monoclonal gammopathy with anti-myelin-associated glycoprotein antibodies. J Neuropathol Exp Neurol 2020;79:1303–1312